INVESTIGATING THE CRATERING HISTORY OF THE SOUTH POLE-AITKEN BASIN.
N. E. Petro[1] and S. C. Mest[2], [1]Planetary Geodynamics Laboratory, Code 698, NASA Goddard Space Flight Center, Greenbelt, MD, 20771. (Noah.E.Petro@nasa.gov); [2]Planetary Science Institute, 1700 E. Ft. Lowell, Suite 106, Tucson, AZ 85719-2395.

Introduction: The South Pole-Aitken Basin (SPA) is known to be the oldest, largest and deepest basin on the lunar surface [1-4]. The enormous size of the basin, with a diameter of ~2600 km and a depth of 8-12 km [2-6], provides exposure of unique lithologies and geochemistries at the surface. These surface compositions are suggestive of lower crustal or upper mantle origin that is unique to the interior of SPA [7-9]. Recently Petro and Pieters [10] described an additional unique aspect of the basin; that the interior of the basin accumulated more material as a result of the formation of large post-basin craters than other areas on the Moon, suggesting a unique cratering history.

Here we examine the cratering history of SPA's interior and compare its history to that of other regions. Using cumulative size-frequency plots we show that the interior of SPA has more large craters (between 60 and ~170 km in diameter) per km^2 than neighboring areas. The greater number of larger craters per km^2 allows for the exposure of deeper material throughout SPA that may contribute to its unique composition.

Definition of Regions: In order to investigate the cratering history of SPA we compare it to that of regions thought to represent ancient crustal compositions [8]. We define two other regions, one centered in the Feldspathic Highlands Terrane (FHT) and one located in the southern nearside highlands (SNH). All of the regions are defined by a radius of 1300 km around a center point [SPA at 180º, 56ºS; FHT at 180º, 56ºN; SNH at 0º, 56ºS]. The locations of the three regions are illustrated in Figure 1.

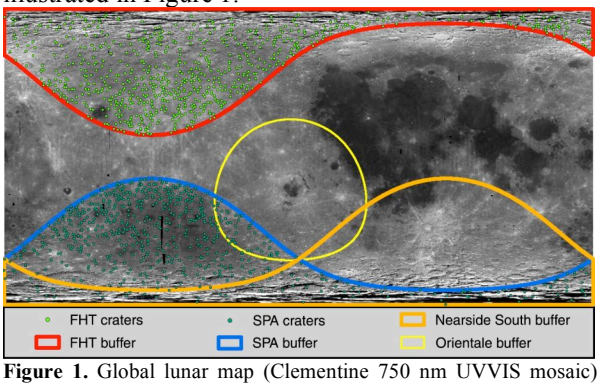

Figure 1. Global lunar map (Clementine 750 nm UVVIS mosaic) showing the locations of impact craters used to determine crater size-frequency distributions used in Figure 2. Buffers are all equal size (radius=1300 km). Projection is Plate-Carree; centered at 0°, -90°.

All three regions contain minimal exposures of mare basalt (~4% of SPA [11], <1% of FHT [e.g. 12,13]), indicating that the dominant modification process acting in these regions is by cratering. One difference between the areas is that the SNH may have been modified by basin-forming impacts to a greater degree than FHT and SPA [8,14]. Ejecta from the Orientale impact may have modified a portion of SPA and SNH [1], as portions of both regions are within 1300 km (~1.8 basin radii) of the Orientale rim as shown in Figure 1. However, in these distal regions larger craters should not have been obliterated by Orientale ejecta.

Crater Database: This study uses groups of craters from two datasets. The first dataset (A) is the Andersson and Whitaker [15] catalogue of named craters [16] (global total of ~8600 craters). While the catalogue is known to be incomplete, particularly for the farside, it is illustrative to use this list as a first-order indicator of variations in cratering histories. Additionally, for this group we only compare SPA to FHT, as any comparison to the nearside using this database will be significantly biased. Efforts are underway to identify all craters greater than 30 km in diameter within the SPA and FHT regions in order to have comparable populations with the southern nearside.

The second dataset (B) used in this study was previously compiled by Petro and Pieters [10] and includes craters Lower Imbrian in age and younger, and larger than 30 km in diameter (411 craters). These craters were identified in the geologic maps in Wilhelms [1], Clementine data by McEwen et al. [17] and Grier et al. [18], and the work of Li [19].

Cumulative Size-Frequency Plots: Cumulative size-frequency plots were prepared for each of the regions using crater datasets A and B. The use of these plots reveals subtle differences between the regions, which may be due to differences in age, inaccuracies in crater identification, or variations in cratering across the lunar surface. In examining dataset A for SPA and FHT, differences in age may be a more important factor as SPA is dominated by pre-Nectarian material while FHT is mostly pre-Nectarian and Nectarian in age. In dataset B, there should not be any variation in the size-frequency plot due to age as all are dominantly older than Lower Imbrian in age [1].

Named craters (dataset A): First, we examine the cratering histories of FHT and SPA to illustrate variations that occur between the regions. The log-log size-frequency plot for these craters is illustrated in Figure 2. Both SPA and FHT have similar frequencies for diameters less than ~60 km. However, at larger diameters, the populations for both regions diverge with SPA containing a larger size-frequency. This trend continues to a diameter of ~170 km; at larger diameters, the frequencies for both regions are roughly the same.

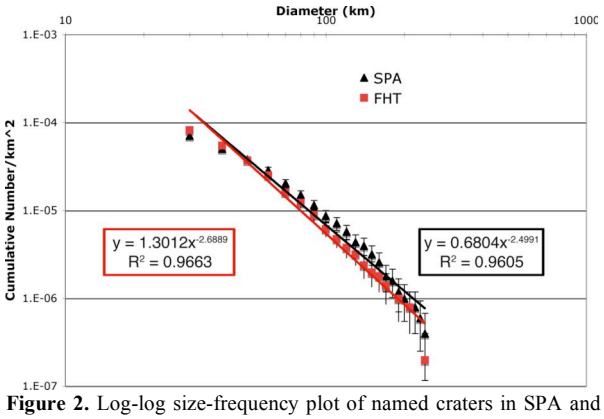

Figure 2. Log-log size-frequency plot of named craters in SPA and FHT. Each region is fit by a power law whose equation is defined in the box highlighted in the matching color.

Post-basin craters (dataset B): Next, we examine the post-basin cratering histories of the three regions to illustrate variations that occur between the regions. The number of post-basin craters within SPA and FHT is ~1/10 the number of named craters described above, yet the size-frequency plots reflect similar trends. A log-log plot of the cumulative size-frequency for dataset B is illustrated in Figure 3. At small diameters (<~60 km) the three regions are broadly similar. At larger diameters SPA diverges and has a greater size-frequency per km^2 than the other regions.

Power law fits of each region (Figure 3) illustrate the offset of SPA craters to higher frequency of craters per km^2. Such an enhancement in cratering frequency would indeed generate the greater amount of accumulated material within SPA compared to the southern nearside and FHT [10].

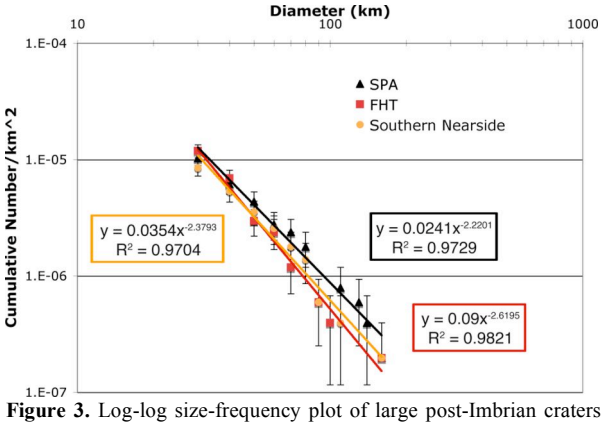

Figure 3. Log-log size-frequency plot of large post-Imbrian craters in SPA, FHT and SNH. Each region is fit by a power law whose equation is defined in the box highlighted in the matching color.

Discussion: In both datasets A and B, the population of large craters within SPA is unique when compared to surrounding regions. In many cases the SPA measurement is within error of the other regions (Figures 2 and 3). This is particularly true for the post-basin craters where the number of craters is small. However, in the named crater population, at large crater diameters, there is little or no overlap in error between FHT and SPA, suggesting that the differences between the regions are not the result of statistical error.

The enhancement in larger craters within SPA is possibly due to larger amounts of pre-Nectarian-aged surfaces within SPA relative to FHT [1] while the enhancement in large post-basin craters is less clear. However, the apparent enhancement in post-basin craters greater than ~60 km diameter (Figure 3) is likely not a result of age differences but may reflect a unique concentration of "recent" large craters. Assuming a 1/10 excavation depth-to-diameter ratio [20], this enhanced concentration of such craters would result in a larger area within SPA having material from depth exposed at the surface. The addition of material from depth within SPA may contribute to or enhance the compositional anomaly prevalent throughout SPA [7-9]. This coupled with the small amount of basin material introduced to the basin's interior [21] may be a reason why the ancient compositional signature is still significant today.

Conclusions: The cratering history of the interior of SPA is unique compared to that of surrounding, ancient regions. The interior of SPA contains a greater number of large (60 to 170 km diameter) named craters (Figure 2) that may reflect older surfaces within SPA when compared to FHT. SPA also has an enhancement in larger post-basin craters relative to FHT and SNH (Figure 3), which may result in an enhancement of the unique composition associated with SPA by the addition of deep (>6 km) material to the basins surface. We will further investigate these apparent relationships by identifying additional craters larger than 30 km in diameter within the three regions and confirming the ages of the post-basin craters (dataset B).

References: [1] Wilhelms, D.E. (1987) The Geologic History of the Moon, 327 pp. [2] Spudis, P.D. (1993) The Geology of Multi-Ring Impact Basins, 263 pp. [3] Spudis, P.D. et al. (1994) *Science*, *266*, 1848. [4] Ryder, G. (2002) *JGR*, *107(E4)*, 6-1. [5] Zuber, M.T. et al. (1994) *Science*, *266*, 1839. [6] Cook, A.C. et al. (2002) *LPS XXXIII*, Abstract #1281. [7] Lucey, P.G. et al. (1998) *JGR*, *103(E2)*, 3701. [8] Joliff, B.L. et al. (2000) *JGR*, *105(E2)*, 4197. [9] Pieters, C.M. et al. (2001) *JGR*, *106(E11)*, 28,001. [10] Petro, N.E. and Pieters, C.M. (2007) *LPS XXXVIII*, Abstract #2069. [11] Yingst, R.A. and Head, J.W. (1997) *JGR*, *102(E5)*, 10,909. [12] Head, J.W. (1975) Origins of Mare Basalts and Their Implications for Lunar Evolution, 66. [13] Gillis-Davis, J.J. et al. (2006) *LPS XXXVII*, Abstract #2454. [14] Petro, N.E. and Pieters, C.M. (2006) *JGR*, *111*, doi:10.1029/2005JE002559. [15] Andersson, L.E. and Whitaker, E.A. (1982) NASA Catalogue of Lunar Nomenclature, 183pp. [16] USGS Gazetteer of Planetary Nomenclature (2008) http://planetarynames.wr.usgs.gov/ [17] McEwen, A.S. et al. (1997) *JGR*, *102*, 9231. [18] Grier, J.A. et al. (2001) *JGR*, *106(E12)*, 32,847. [19] Li, L. (2002) Lunar Crustal Mixing and Compositional Contamination, Brown University. [20] Stöffler, D. et al., (2006) New Views of the Moon, 519. [21] Petro, N.E. and Pieters, C.M. (2004) *JGR*, *109*, doi:10.1029/2003JE002182.

Acknowledgements: This work is supported by the NASA Postdoctoral Program under the administration of Oak Ridge Associated Universities (ORAU).